

# LGGNet: Learning from Local-Global-Graph Representations for Brain-Computer Interface

Yi Ding, *Student Member, IEEE*, Neethu Robinson, *Member, IEEE*, Qiuhaio Zeng,  
and Cuntai Guan, *Fellow, IEEE*

**Abstract**—In this paper, we propose LGG, a neurologically inspired graph neural network, to learn local-global-graph representations from Electroencephalography (EEG) for a Brain-Computer Interface (BCI). A temporal convolutional layer with multi-scale 1D convolutional kernels and kernel-level attention fusion is proposed to learn the temporal dynamics of EEG. Inspired by neurological knowledge of cognitive processes in the brain, we propose local and global graph-filtering layers to learn the brain activities within and between different functional areas of the brain to model the complex relations among them during the cognitive processes. Under the robust nested cross-validation settings, the proposed method is evaluated on the publicly available dataset DEAP, and the classification performance is compared with state-of-the-art methods, such as FBFgMDM, FBTSC, Unsupervised learning, DeepConvNet, ShallowConvNet, EEGNet, and TSception. The results show that the proposed method outperforms all these state-of-the-art methods, and the improvements are statistically significant ( $p < 0.05$ ) in most cases. The source code can be found at: <https://github.com/yi-ding-cs/LGG>

**Index Terms**—Deep learning, electroencephalography, graph convolutional neural networks.



## 1 INTRODUCTION

RAIN-computer interface (BCI) enables human brains to communicate with machines directly using Electroencephalography (EEG) [1]. Several electrodes are placed on the surface of the human head to collect EEG signals. A typical BCI system consists of a data acquisition module, a pre-processing module, a classification module, and a feedback module [2]. BCI has a wide range of applications in the real world, such as robot controlling [3], stroke rehabilitation [4], and emotion regulation for mental disorders [5]. Among various BCI applications, emotion recognition via EEG has huge potentials in Cognitive Behavioural Therapy (CBT) [6], Emotion Regulation Therapy (ERT)/Emotion-Focused Therapy (EFT) [7] [8] by enabling artificial intelligence (AI) to identify human emotions. Recently, EEG emotion recognition has caught the attention of researchers [9] [10]. Zheng *et al.* [11] proposed a discriminative graph regularized extreme learning machine with differential entropy features of EEG for emotion recognition. Li *et al.* [12] designed brain networks with phase-locking value to detect emotions from multiple features of EEG. Li *et al.* [13] explored the effect of multiple features from EEG for cross-subject emotion recognition. Liang *et al.* [14] proposed an unsupervised clustering method based on multiple types of EEG features to classify emotions. Compared with transitional machine learning methods, deep learning methods have shown promising results in BCI domain, such as motor imagery classification [15] [16] [17] [18], emotion recognition [19] [20] [21], and mental-task classification [22] [23]. Yang *et al.* [24] designed a neural network with sub-network nodes

for EEG emotion recognition. Li *et al.* [19] constructed EEG into 2D images and proposed a Hierarchical Convolutional Neural Networks (HCNN) to extract the spatial pattern of the EEG. Although many machine/deep learning methods have been proposed for emotion recognition, most of them highly rely on the manually extracted EEG features. With the feature extracting ability of Convolutional Neural Networks (CNNs), learning from EEG signals directly becomes reliable. Schirmer *et al.* [15] proposed deep and shallow convolutional neural networks, named DeepConvNet and ShallowConvNet, to process EEG data. Lawhern *et al.* [18] proposed EEGNet, an end-to-end deep learning framework that uses three convolutional layers to extract the temporal and spatial patterns from EEG data. Ding *et al.* [21] designed TSception that utilizes multi-scale convolutional kernels to learn discriminative representations from affective EEG signals.

EEG signals contain abundant brain activity information in different frequency bands [25]. To extract more information-rich representations from EEG, a temporal convolutional layer with multi-scale 1D convolutional kernels is adopted as TSception. A kernel-level attention fusion layer is further designed to fuse the learned temporal representations with attention. For spatial information, EEG signals can be naturally regarded as graph-structured data, with each electrode being the node and spatial relations or functional connections being the edges. The brain is a complex network with a hierarchical spatial and functional organization at the level of neurons, local circuits, and functional areas [26]. 1D convolutional kernels along the spatial dimension of EEG [15] [18] might not be able to capture the complex relations among different local and global brain functional areas. Although TSception has a hemisphere kernel to learn the relations among hemispheres, the relations among different functional areas of

- Yi Ding, Neethu Robinson, Qiuhaio Zeng, and Cuntai Guan are with the School of Computer Science and Engineering, Nanyang Technological University, 50 Nanyang Avenue, Singapore, 639798.  
E-mail: (ding.yi, nrobinson, qiuhaio.zeng, ctguan)@ntu.edu.sg.

Cuntai Guan is the Corresponding Author.

the brain are not extracted effectively. To address the above problems, we define the EEG data as a local-global graph whose local graphs belong to the different functional areas of the brain according to neurological knowledge [26] [27]. The nodes in each local graph are fully connected because they reflect the brain activities within each brain functional area. Emotions are high-order cognitive process with the interplay of more basic processes in perceptual, attentional, and mnemonic systems that are not unique to emotion. Activating one particular brain region also tends to activate other regions in the group [28]. The edges of local graphs, or the global connections among local graphs, reflect the complex functional connections among different brain functional regions. Inspired by DGCNN [29] that utilizes a learnable adjacent matrix in the graph convolutional layer, the global connections are learnable via back-propagation during the training process instead of defining the connections manually. Hence, we can also explore the complex connection patterns by deep learning. Besides, according to psychophysiological evidence [27], the left and right halves of the human frontal brain areas differentially associate with particular emotions. The frontal region is further divided into smaller local regions which are symmetrically located on the left and right hemispheres to learn more emotion-related local-global representations.

To evaluate the proposed method, learning Local-Global-Graph representations (LGG), we conduct emotion classification experiments on the publicly available benchmark dataset, a Database for Emotion Analysis using Physiological signals (DEAP) [30]. The proposed LGG is compared with several state-of-the-art methods in the BCI domain, namely FBFgMDM [31], FBTSC [31], Unsupervised learning [14], DeepConvNet [15], ShallowConvNet [15], EEGNet [18], and TSception [21]. From the experiment results, LGG achieves significantly ( $p < 0.05$ ) higher accuracy than other methods. Furthermore, ablation studies are conducted to understand the importance of local and global graph-filtering layers in LGG. Extensive experiments are conducted to study the effect of the number of temporal kernels in the temporal convolutional layers and different local-global graph definitions. After that, we also visualize the most informative region of the data identified by the network during training by utilizing saliency maps [32].

The major contribution of this work can be summarised as:

- Propose LGG, a neurologically inspired graph neural network, to learn local-global-graph representations from EEG.
- The proposed method is compared with several state-of-the-art methods in the BCI field, namely FBFgMDM [31], FBTSC [31], DeepConvNet [15], ShallowConvNet [15], EEGNet [18], and TSception [21].
- Conduct extensive ablation studies and analysis experiments to better understand LGG.

The PyTorch implementation of LGG is available at: <https://github.com/yi-ding-cs/LGG>

The remainder of this article is organized as follows. Some related work will be introduced in Section II. In Section III, the proposed LGG is introduced. In Section IV,

the dataset and experiment settings will be introduced. The result and analysis will be given in Section V. Finally, we discuss and come to conclusions in Section VI and Section VII respectively.

## 2 RELATED WORK

### 2.1 Different Representations of EEG data

EEG data can be treated as 2D signals whose dimensions are channels (EEG electrodes) and time respectively. The channel in this paper refers to the EEG electrodes instead of RGB dimensions in images or the input/output channels for convolutional layers if not specified. The channel dimension reflects the brain activities across different functional areas because the electrodes are located at different areas on the surface of the human's head. The time dimension contains the changes in brain activities over time. There are three main types of EEG representations in recent studies, namely 2D time series, images, and graphs.

2D time-series representation is the most commonly used format in deep learning methods. In these works, there are typically temporal convolutional layers to extract temporal information channel by channel and spatial convolutional layers to extract spatial information. Schirrmester *et al.* [15] proposed deep and shallow convolutional neural networks, named DeepConvNet and ShallowConvNet, to process EEG data. Robinson *et al.* [33] presented a deep learning-driven EEG-BCI system to perform decoding of hand motor imagery using CNNs. Lawhern *et al.* [18] proposed EEGNet, which extracts spatial information by the depth-wise convolution kernel whose size is  $(n, 1)$ . The global spatial dependency can be learned if  $n$  equals the number of channels.

Another type of EEG representation is the image. In these works, the electrodes are rearranged into a 2D map according to their relative locations on the brain surface, and the raw data or features of each electrode will be the third dimension of the 2D map. Li *et al.* [19] used the relative locations of the electrodes to rearrange the channel dimension of EEG to map each channel on a sparse 2D location map. Siddharth *et al.* [34] applied pre-trained VGG-16 on the EEG-PSD-image features for emotion recognition tasks. These image-liked representations can reflect the spatial pattern of the EEG. Hence,  $(n, n)$  sized convolutional kernels can be applied to them as the typical convolution on images. The local spatial patterns are captured through sharing kernels. However, one of the obvious drawbacks is that the global spatial information is not well extracted since  $n$  is usually small which reduces the perception range.

Recently, more and more studies represent EEG data as graphs. In these works, EEG data are treated as graphs, with the electrodes being the node and spatial distance or correlations being the edges. Song *et al.* [29] proposed dynamic graph convolutional neural networks for EEG emotion recognition with a trainable adjacency matrix. Jang *et al.* [35] defined the connections as both spatial locations and correlations among electrodes to do video classification via EEG graphs. Zhong *et al.* [36] defined the adjacency matrix according to the spatial distance and added some global connections according to asymmetry in neuronal activities.

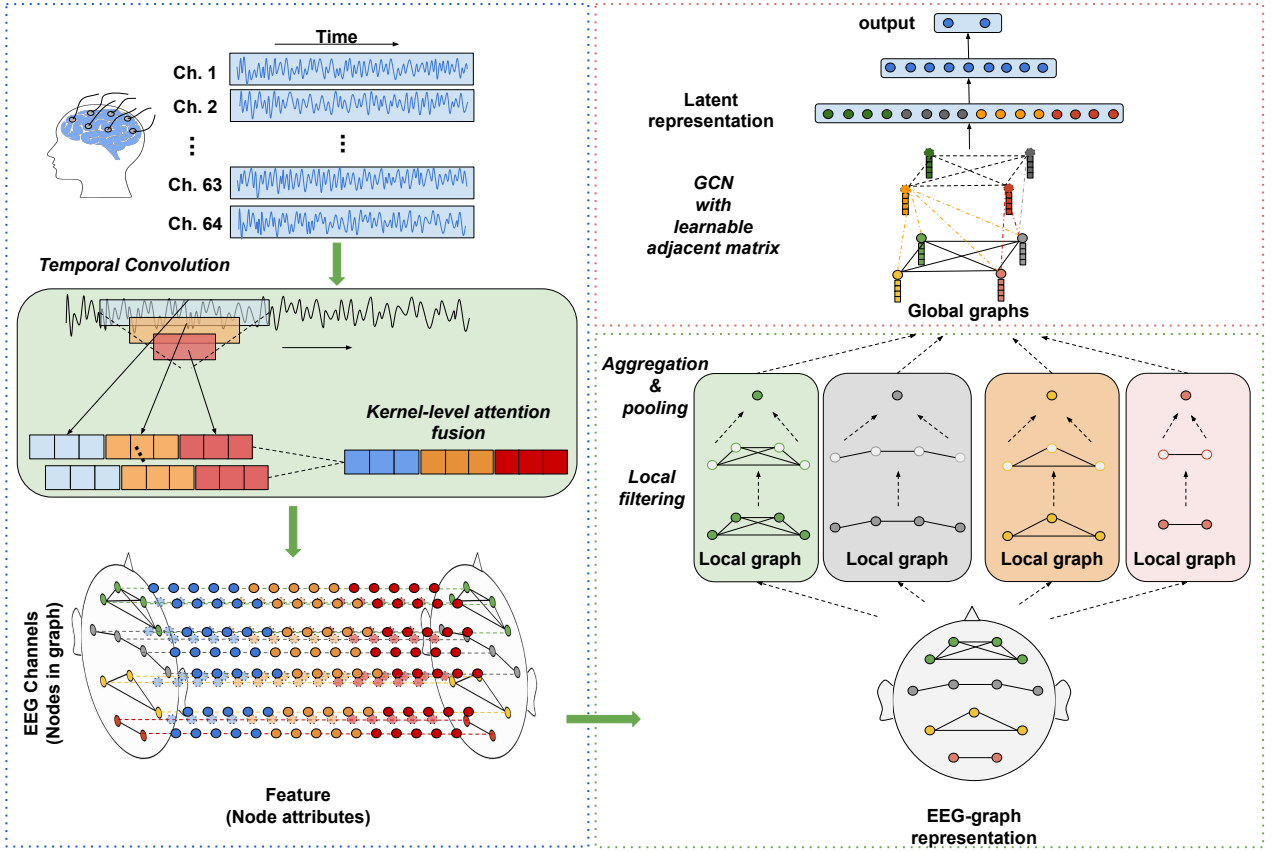


Fig. 1. Structure of LGG. LGG has three main parts, temporal convolutional layer, local graph-filtering layer, and global graph-filtering layer respectively. The temporal convolutional layer aims to learn dynamic frequency representations from EEG directly instead of human extracted features. The local graph-filtering layer learns the brain activities within each local region. Then the global graph-filtering layer with a trainable adjacency matrix will be applied to learn complex relations among different local regions. Four local graphs are shown in the figure for illustration purposes only, the detailed local-global-graph definitions are provided in subsection ‘Local-Global-Graph Representation of EEG’ of section III. Best viewed in color.

## 2.2 Graph Convolutional Neural Networks

A graph is represented as  $\mathcal{G} = (\mathcal{V}, \mathcal{E})$ , where  $\mathcal{V}$  is the set of nodes, and  $\mathcal{E}$  is the set of edges.  $v_i \in \mathcal{V}$  denotes a node, and  $e_{i,j} = (v_i, v_j) \in \mathcal{E}$  denotes an edge. The adjacency matrix  $A$  is derived as a  $n \times n$  matrix with  $A_{i,j} = 1$  if  $e_{i,j} \in \mathcal{E}$  and  $A_{i,j} = 0$  if  $e_{i,j} \notin \mathcal{E}$ . A graph, also known as attributed graph, may have node attributes  $X$ , where  $X \in \mathbb{R}^{n \times d}$  is a node feature matrix with  $\mathbf{x}_v \in \mathbb{R}^d$  representing the feature vector of a node  $v$ . A graph can be a directed graph or an undirected one. The adjacency matrix of a directed graph may not be asymmetric, if a single direction connection exists. (e.g.,  $e_{i,j} \neq e_{j,i}$ ). The adjacency matrix of an undirected graph is symmetric, and  $A = A^T$ . Graph Neural Networks (GNNs) [37] were proposed to deal with the graph structured data. Graph Convolutional Neural Networks (GCNN) [38] extended the convolution operation to graph in the spectral domain. It can generate a node representation by aggregating its features and neighbors’ features. Kipf *et al.* [39] proposed a scalable graph convolution neural network, which can encode both local graph structure and the feature of the node with improved computational efficiency. In this work, the global graph is defined as an undirected graph of local sub-areas. After filtering on local graphs, the GCN [39] with a trainable adjacency matrix will be applied to extract

the complex relations among different local graphs.

## 3 LGG FOR BCI

In this section, the proposed method, learning Local-Global-Graph representations (LGG), will be introduced. The notations used in this paper are illustrated in Table 1. Graph representations of EEG are constructed first with neuroscience-inspired graph structures, after which LGG will be used to learn local-global-graph representations from the EEG graphs. As shown in Fig. 1, LGG has three main parts, a temporal convolutional layer, a local graph-filtering layer, and a global graph-filtering layer respectively. The temporal convolutional layer aims to learn dynamic frequency representations from EEG directly instead of human extracted features. The local graph-filtering layer learns the brain activities within each local region, after which the global graph-filtering layer with a trainable adjacency matrix will be applied to learn complex relations among different local regions.

### 3.1 Local-Global-Graph Representation of EEG

In this section, two types of local-global-graph representations are constructed based on neuroscience findings

TABLE 1  
Notations used in this paper

Symbol	Description
$\mathcal{G}_g, \mathcal{G}_a$	general and affective graphs
$\mathbf{X}_n$	EEG samples
$i$	index of EEG samples
$c$	number of EEG channels
$l$	length of the EEG sample in time dimension
$j$	index of EEG channels
$A_{local}, A_{global}$	local and global adjacent matrix
$k$	index of temporal kernel levels
$f$	length of features
$L$	maximum value of temporal kernel levels
$\alpha$	ratio coefficient of temporal kernel sizes
$S_T^k$	temporal kernel sizes
$\Phi(\cdot)$	activation functions
$\mathbf{Z}$	output tensor of a neural network layer
$\mathcal{F}(\cdot)$	operations
$\Gamma(\cdot)$	concatenation of tensors
$\mathbf{W}$	trainable weight matrix
$\mathbf{b}$	trainable bias vector
$\circ$	Hadamard product
$p, P$	index and number of local graphs
$q, Q$	index and number of nodes in a local graph
$m$	index of GCN layers
$h$	length of the hidden output of GCN layers
$\Upsilon(\cdot)$	flatten operation

The order of the symbols is the same as their appearance sequence

[26] [28] [27], namely general graph  $\mathcal{G}_g$  and affective graph  $\mathcal{G}_a$ . Let  $\mathbf{X}$  denote the EEG input sample array.  $\mathbf{X} = [\mathbf{X}_1, \dots, \mathbf{X}_n], \mathbf{X}_n \in \mathbb{R}^{c \times l}$ , where  $n$  is the number of EEG samples,  $c$  is the number of channels, and  $l$  is the length of each sample. For one EEG sample  $\mathbf{X}_i = [x_1, x_2, \dots, x_j]^T, x_j \in \mathbb{R}^{1 \times l}, j \in (1, 2, \dots, c)$ , each electrode is regarded as one node in the EEG graph, and the EEG signal of each electrode  $x_j$  is regarded as the attribute of the  $j$ -th node. To learn more information on graph data, the adjacent relations among nodes are very important. To effectively define adjacent relations, several neuroscience findings are taken into consideration. Human brains have several functional regions which will be active during different cognition processes [26]. A well-known definition of functional regions is the frontal lobe, parietal lobe, temporal lobe, and occipital lobe [9]. EEG is collected from the electrodes located on the surface of the brain, catching activities of different functional areas. They are placed according to the 10-20 system [9]. Hence, we define the local graph based on the different functional areas on the brain according to the 10-20 system. The general local-global-graph definition,  $\mathcal{G}_g$  is shown in Fig. 2. LGG using the general local-global-graph definition is regarded as LGG-G and may be used for any BCI classifications. LGG-G is also used as a specific version of LGG for performance comparison.

The frontal lobe is the largest portion of the brain, and it is responsible for high-level behaviours, such as thinking, attention, and emotions [26]. Distinguishable asymmetries exist across numerous nodes in the network of brain areas involved in emotion, particularly within the frontal area [28]. To learn the discriminative asymmetry pattern of emotions, the frontal area is further split into several smaller

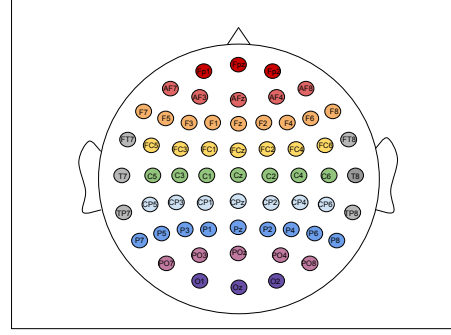


Fig. 2. General local-global-graph definition. This local graph structure is defined according to the 10-20 system. Each local graph reflects the brain activities of a certain brain functional area. The nodes in a local graph are in the same color. This diagram illustrates the definition for the 62 channel EEG.

local graphs which are symmetrically located on the left and right frontal hemispheres as [40]. The affective local-global graph,  $\mathcal{G}_a$  is shown in Fig. 3.

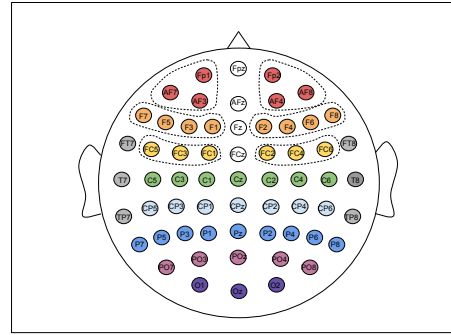


Fig. 3. Affective local-global-graph definition. Based on the general local-global graph, the neuroscience evidence of emotional asymmetry pattern in frontal areas is further considered. Six frontal local graphs that are symmetrically located on the left and right frontal area of the brain are added to learn emotional asymmetry patterns. To learn the asymmetry patterns better, the electrodes on the central line (in white) are removed.

After defining the local-global graphs, the local-global connection among them will be defined. For both the general graph and affective graph, the electrodes within one local graph are fully connected because we hold the hypothesis that different sub-group electrodes can reflect the similar brain activities of the corresponding functional areas. The local adjacent matrix  $A_{local}$  is defined as:

$$A_{local} = \begin{bmatrix} 1 & \cdots & 1 \\ \vdots & \ddots & \vdots \\ 1 & \cdots & 1 \end{bmatrix} \quad (1)$$

where all elements are 1. The size of the  $A_{local}$  depends on how many channels are within the local graph.

Emotion is a high-level cognitive process that will involve several basic cognitive processes. These processes are not unique to emotion. Activating one particular brain region also tends to activate other regions in the group [28]. Hence we hold the hypothesis that the local graphs are not independent during emotional processes. Due to the complex relations among brain functional areas, the global

connections are set to be learnable via back-propagation during the networks training process [29] instead of manually defined one. We assume the global connection is undirected. The adjacent matrix of the global graph,  $\mathbf{A}_{global}$ , is symmetric and can be defined as:

$$\mathbf{A}_{global} = \begin{bmatrix} w_{1,1} & \cdots & w_{1,n} \\ \vdots & \ddots & \vdots \\ w_{1,n} & \cdots & w_{n,n} \end{bmatrix} \quad (2)$$

where  $w_{1,n}$  are the trainable parameters.

### 3.2 Temporal Convolutional Layer

The temporal convolutional layer is designed to learn dynamic temporal information from the EEG signal (node attributes of EEG graph) of each electrode (node of EEG graph). It has two main parts, namely the multi-scale temporal convolutional layer and kernel-level fusion layer. The multi-scale temporal convolutional layer consists of multi-scale 1D temporal kernels (T kernels). In order to learn dynamic-frequency representations, the length of the temporal kernels is set in different ratios of the sampling rate  $f_s$  [21]. The ratio coefficient is denoted as  $\alpha^k \in \mathbb{R}$ , where  $k$  is the level of the temporal convolutional layer.  $k$  will vary from 1 to  $L$  ( $\alpha = 0.5, L = 3$ , in our study). Hence,  $S_T^k$ , the size of T kernels in  $k$ -th level, can be defined as:

$$S_T^k = (1, \alpha^k \cdot f_s), k \in [1, 2, 3] \quad (3)$$

Multi-scale 1D temporal convolutional kernels can enrich the learned dynamic time-frequency representations of EEG [21]. The information of EEG signals can be reflected in different frequency bands [25]. If EEG is fed into LGG directly, those multi-scale 1D temporal kernels serve as dynamic-frequency representation learners. Those multi-scale temporal kernels will extract dynamic temporal representations of EEG in different frequency bands if the band-passed EEG signal is used as the input of LGG.

Given EEG data  $\mathbf{X}_i \in \mathbb{R}^{c \times l}$ ,  $i \in [1, \dots, n]$ , where  $n$  is the number of EEG samples,  $c$  is the number of channels, and  $l$  is the length of each sample, the multi-scale temporal kernels will be applied parallelly to learn dynamic temporal/frequency representations. The learned representations will be further activated by  $\Phi_{LeakyReLU}(\cdot)$  function, after which the activated representations will be further down-sampled by average pooling. Let  $\mathbf{Z}_{conv}^k$  denote the output of the  $k$ -th level temporal kernel,  $\mathbf{Z}_{conv}^k \in \mathbb{R}^{t \times c \times f_k}$ , where  $t$  is the number of each level's T kernel,  $c$  is the number of channels,  $f_k$  is the length of the feature after  $k$ -th level convolution operation.  $\mathbf{Z}_{temporal}^k$  is defined as:

$$\mathbf{Z}_{temporal}^k = \mathcal{F}_{AvgPool}(\Phi_{LeakyReLU}(\mathcal{F}_{Conv1D}(\mathbf{X}_i, S_T^k))) \quad (4)$$

where  $\mathcal{F}_{Conv1D}(\mathbf{X}_i, S_T^k)$  is convolution operation using T kernel of size  $S_T^k$  on  $\mathbf{X}_i$ , and  $\mathcal{F}_{AvgPool}$  is the average pooling operation.

The output of all levels' T kernel will be concatenated along feature dimension. Then batch normalization [41] is utilized to reduce the internal covariate shift effects in neural networks. Hence, the output of the multi-scale temporal convolutional layer  $\mathbf{Z}_{multi-scale}^i$  for  $\mathbf{X}_i$  can be calculated by:

$$\mathbf{Z}_{multi-scale}^i = \mathcal{F}_{bn}(\Gamma(\mathbf{Z}_{temporal}^1, \dots, \mathbf{Z}_{temporal}^k)) \quad (5)$$

where the  $\mathcal{F}_{bn}$  is the batch normalization function, and  $\Gamma(\cdot)$  stands for concatenation operation along the feature (f) dimension.

After concatenation of the output from different level T kernels, a one-by-one convolutional layer is adopted as a kernel-level attention fusion layer to fuse the features learned by different kernels to get the final temporal representations of each  $\mathbf{X}_i$ ,  $\mathbf{Z}_{T-fuse} \in \mathbb{R}^{c \times \sum f_k}$ , as:

$$\mathbf{Z}_{T-fuse}^i = \mathcal{F}_{squeeze}(\mathcal{F}_{fuse}(\mathbf{Z}_{multi-scale}^i)) \quad (6)$$

where  $\mathcal{F}_{fuse}$  is the one-by-one convolution function, and the  $\mathcal{F}_{squeeze}$  removes the empty dimension of the output from the one-by-one convolution.

### 3.3 Local Graph-Filtering Layer

Local graphs reflect the brain activities of a certain functional area. Hence, the nodes in the local graph are fully connected. In order to learn the local brain activities, a local graph-filtering matrix will be utilized on the learned representations from temporal convolutional layers. There are two steps in the local graph-filtering layer: local graph filtering and local representation aggregating. Given the trainable local graph-filtering matrix  $\mathbf{W}_{local} \in \mathbb{R}^{c \times \sum f_k}$ , and local graph-filtering bias vector  $\mathbf{b}_{local} \in \mathbb{R}^{c \times 1}$ , the local graph-filtering weights will be assigned to the representation of each electrode by:

$$\mathbf{Z}_{filtered}^i = \mathcal{F}_{AvgPool}(\Phi_{ReLU}(\mathbf{W}_{local} \circ \mathbf{Z}_{T-fuse}^i - \mathbf{b}_{local})) \quad (7)$$

where  $\circ$  is the Hadamard product.

After local graph filtering, the filtered representation within each local graph will be aggregated by an aggregating function  $\mathcal{F}_{aggregate}(\cdot)$ . Let  $\mathbf{Z}_{filtered}^i = [\mathbf{Z}_1', \dots, \mathbf{Z}_p']^T$ ,  $p \in [1, P]$  be the locally filtered graph representations, where  $\mathbf{Z}_p' \in \mathbb{R}^{c' \times f'}$  is the local-graph representation,  $P$  is the total number of local graphs,  $c'$  is the number of nodes in the local graph ( $\sum c_p' = c$ ), and  $f'$  is the feature length of each node after local graph filtering. A local graph can be denoted as:  $\mathbf{Z}_p' = [z_1^q, \dots, z_p^q]^T$ ,  $q \in [1, Q]$ , where  $z_p^q$  is the node vector in the local graph, and  $Q$  is the total number of nodes in the local graph. The aggregating function will aggregate the node vectors within each local graph. It can be maximum, minimum, average, etc. In this paper, the average operation is selected as the aggregating function. Hence, the output of the local graph-filtering layer,  $\mathbf{Z}_{local}^i$  can be calculated by:

$$\begin{aligned} \mathbf{Z}_{local}^i &= \mathcal{F}_{aggregate}(\mathbf{Z}_{filtered}^i) \\ &= \mathcal{F}_{aggregate}([\mathbf{Z}_1', \dots, \mathbf{Z}_p']^T) \\ &= [\frac{1}{Q} \sum_{q=1}^Q z_1^q, \dots, \frac{1}{Q'} \sum_{q=1}^{Q'} z_p^q]^T \end{aligned} \quad (8)$$

where  $p$  is the index of local graphs,  $q$  is the index of nodes in each local graph, and  $Q$  is the number of nodes in a certain local graph.  $Q$  might or not equal to  $Q'$ , since the number of node in different local graphs might not be the same.

### 3.4 Global Graph-Filtering Layer

The global graph represents the complex relations among different brain functional areas by the adjacent patterns in the graph representations of EEG. Instead of manually defining the fixed adjacent matrix, a learnable adjacent matrix is utilized to learn the complex relation pattern via back-propagation. Given the learnable adjacent matrix,  $A_{global} \in \mathbb{R}^{p \times p}$  described in Eq.2, the simple GCN [39] layer is adopted to learn the global-graph representations. Let the nonlinear projecting weight matrix of  $m$ -th GCN layer be  $W_m \in \mathbb{R}^{f' \times h}$ , where  $h$  is the length of the hidden output after GCN, and the trainable bias vector be  $\mathbf{b}_m \in \mathbb{R}^{p \times 1}$ , the output of  $m$ -th GCN layer can be calculated as:

$$\mathbf{Z}_m = \Phi_{ReLU}(A\mathbf{Z}_{m-1}W_m - \mathbf{b}_m) \quad (9)$$

where  $m$  is the index of GCN layers, and  $A$  is the adjacent matrix.

Before the global graph filtering, batch normalization,  $\mathcal{F}_{bn}(\cdot)$ , is applied to avoid internal covariant shift issue. In this paper, the number of global GCN layers is set to be one. Let the nonlinear projecting weight matrix of GCN layer be  $W_{global} \in \mathbb{R}^{f' \times h}$ , where  $h$  is the length of the hidden output after GCN, and the trainable bias vector be  $\mathbf{b}_{global} \in \mathbb{R}^{p \times 1}$ . The global-graph filtering of  $\mathbf{Z}_{local}^i$  can be calculated by:

$$\mathbf{Z}_{global}^i = \Phi_{ReLU}(A_{global}(\mathcal{F}_{bn}(\mathbf{Z}_{local}^i)W_{global} - \mathbf{b}_{global})) \quad (10)$$

After getting the globally filtered representation, the flattened representation will be fed into a linear layer to generate the final output as:

$$Output = \Phi_{softmax}(W\mathcal{F}_{dropout}(\Upsilon(\mathbf{Z}_{global}^i)) + \mathbf{b}) \quad (11)$$

where the  $\Upsilon(\cdot)$  is the flatten operation,  $W$  is the trainable weight matrix, and  $\mathbf{b}$  is the bias term.

Finally, the proposed LGG can be summarized in Algorithm 1

## 4 EXPERIMENTS

### 4.1 Datasets

LGG is evaluated on a publicly available dataset, a Database for Emotion Analysis using Physiological signals (DEAP) [30]. It is a multi-modal human affective states dataset, including EEG, facial expressions, and galvanic skin response (GSR). The dataset is available on this website<sup>1</sup>. 40 emotional music videos are carefully selected as the stimuli to induce different emotions to the subject. Each video lasts for 1 min. Before each trial, there is a 3 seconds' baseline recording stage. An online self-assessment tool is designed to collect the feedback of subjects on arousal, valence, dominance, and liking. For each dimension, a continuous 9-point scale was adopted to measure the level of those dimensions. 32 subjects participated in the data collection experiments. During the experiment, EEG, GSR, and facial expressions are recorded. A 32-channel EEG collecting device is used with the sampling rate being 512Hz.

1. <http://www.eecs.qmul.ac.uk/mmv/datasets/deap/index.html>

---

### Algorithm 1: LGG

---

**Input:** EEG data  $X_i \in \mathbb{R}^{c \times l}$ ; ground truth label  $y$ ;  
graph definitions  $\mathcal{G}_g$  and  $\mathcal{G}_a$ ; trainable global adjacent matrix  $A_{global}$   
**Output:**  $pred$ , the prediction of LGG

- 1 Initialization;
- 2 # get the output of the temporal convolutional layer **for**  
   $j \leftarrow 1$  **to** 3 **do**
- 3   | get  $j$ -th temporal kernel size by Eq. 3;
- 4   | get  $\mathbf{Z}_{temporal}^j$  by Eq. 4 using  $X_i$  as input;
- 5 **end**
- 6 get  $\mathbf{Z}_{multi-scale}^i$  by Eq. 5;
- 7 do kernel-level attention fusion by Eq. 6 to get  
   $\mathbf{Z}_{T-fuse}^i$ ;
- 8 # get the output of the local graph-filtering layer
- 9 do local filtering on each node attribute by Eq. 7;
- 10 aggregate the filtered node attribute within each  
  local graph ( $\mathcal{G}_g$  or  $\mathcal{G}_a$ ) by Eq. 8;
- 11 # get the output of the global graph-filtering layer
- 12 do global filtering on embeddings of local graphs by  
  Eq. 10 with  $A_{global}$ ;
- 13 get  $pred$  by Eq. 11;

**Return:**  $pred$

---

### 4.2 Pre-processing

Deep learning can learn from EEG data directly instead of using human extracted features [18] [15] [21]. Hence, EEG data with several pre-processing operations are used as the input samples of the neural networks. First, the 3 seconds' pre-trial baseline was removed from each trial. After that, the data were down-sampled to 128Hz. Electrooculogram (EOG) was removed using the method described in [30]. A band-pass filter was applied to remove the signals which are lower than 4Hz and higher than 45Hz. Average reference was conducted on the filtered data to get the final pre-processed data. The label for each dimension is a continuous 9-point scale. To divide each dimension into high/low classes, we set 5 as the threshold to project the 9 discrete values into low and high classes in each dimension as [30] [31]. In this study, arousal, valence, and liking dimensions are considered since some subjects' dominance dimension has a single class after label projection. The reprocessed data will be fed into the deep learning methods directly.

Besides, if 5 is selected as the threshold of high and low classes for the DEAP dataset, the classes will become unbalanced, which will cause chance level shifting issue for accuracy. Adopting the suggestion from [31], we randomly duplicated the sample of the smaller class to make the classes balanced so that the chance level becomes 50%.

### 4.3 Experiment Settings

To avoid testing data leakage problems, we follow [31], a leave-one-trial-out cross-validation for subject-specific experiments is adopted to evaluate the proposed LGG. One trial's data is used as the input to the neural networks as [31]. Each time, one trial is used as testing data, the others are used as training data. For the training data, a 5-fold cross-validation is adopted to train a model to form

TABLE 2  
Comparison against classification accuracy on leave one trial out experiments with FBFgMDM, FBTS, Unsupervised learning, EEGNet, DeepConvNet, ShallowConvNet, TSception on DEAP

Method	Arousal	std	Valence	std	Liking	std
FBFgMDM [31]	60.04% ***	–	61.01% *	–	–	–
FBTS [31]	60.60% ***	–	61.09% *	–	–	–
Unsupervised learning [14]	61.17% ***	–	54.61% ***	–	65.08% ***	–
DeepConvNet [15]	72.21% ***	13.56%	62.80% *	11.79%	74.33% ***	12.88%
ShallowConvNet [15]	72.39% ***	11.41%	63.02% *	11.88%	74.01% ***	12.97%
EEGNet [18]	74.03% ***	14.98%	66.25%	13.67%	76.71% *	13.72%
TSception [21]	77.37% *	12.99%	66.06%	13.09%	77.00% *	16.87%
<b>LGG-G(ours)</b>	<b>79.59%</b>	<b>15.37%</b>	<b>65.68%</b>	<b>16.01%</b>	<b>78.70%</b>	<b>19.08%</b>
<b>LGG-A(ours)</b>	<b>80.90%</b>	<b>15.95%</b>	<b>69.34%</b>	<b>14.58%</b>	<b>81.88%</b>	<b>18.30%</b>

$p$ -value between the method and LGG-A: \* indicating ( $p < 0.05$ ), \*\* indicating ( $p < 0.01$ ), \*\*\* indicating ( $p < 0.001$ ).

LGG-G: LGG using general local-global graph

LGG-A: LGG using affective local-global graph

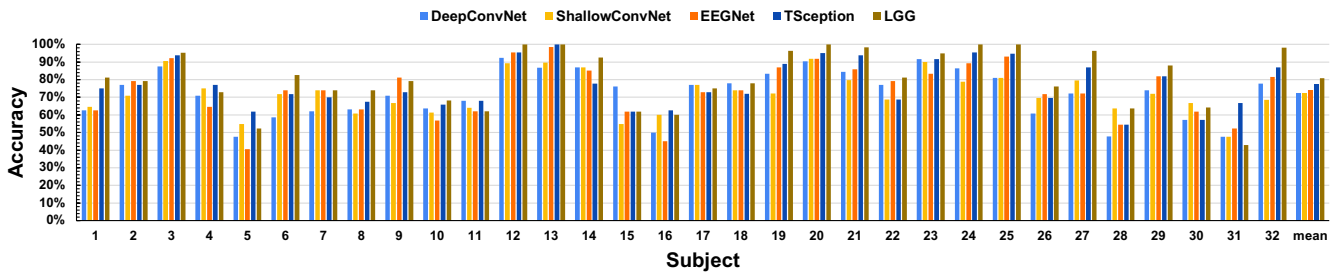


Fig. 4. Mean accuracy of each subject for arousal on DEAP. LGG refers to LGG-A

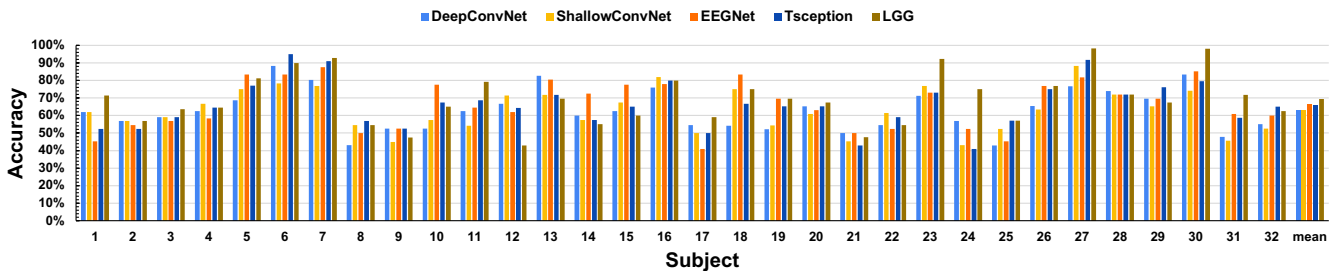


Fig. 5. Mean accuracy of each subject for valence on DEAP. LGG refers to LGG-A.

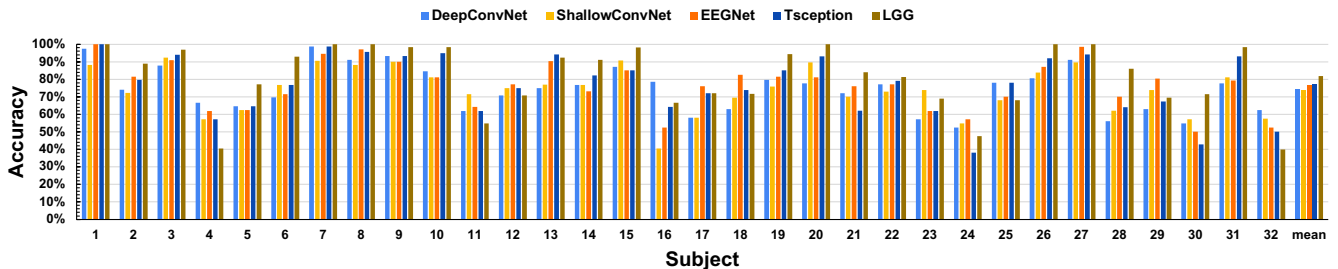


Fig. 6. Mean accuracy of each subject for liking on DEAP. LGG refers to LGG-A



a more robust nested cross-validation [42]. The outer loop of the nested cross-validation is the leave-one-trial-out, and the inner loop is the 5-fold cross-validation. This process is repeated until each trial’s data has been used as testing data once. The average accuracy and standard deviation of all subjects are reported as the final evaluation criterion as [31] [30]. In the inner loop, a two-stage training strategy is utilized as well to make full use of the training data. More details about the two stages training process will be provided in the next section.

#### 4.4 Two-stage Training

To make full use of the training data, for each step of leave-one-trial-out cross-validation, the neural networks are trained in two stages using the training data. Since the inner loop of the nested cross-validation is the 5-fold cross-validation, 20% of the training data is utilized as validation data in each step of the 5-fold cross-validation. First, the best performing model in 5 fold is saved as the candidate for testing. Then all 5 folds of the training data are combined as the new training data. The candidate model will be fine-tuned for 5 epochs on the combined training data with a smaller learning rate compared with the first stage training. After getting the fine-tuned model, it will be evaluated on the testing data. Testing data is never used in any form during the training process to avoid biased evaluation.

#### 4.5 Implementation Details

The code is implemented using PyTorch [43] library, and the source code can be found via this link<sup>2</sup>.

The number of temporal kernels in the temporal convolutional layer is equal to 5. The numbers of local graphs are 11 and 13 for general local-global graph  $\mathcal{G}_g$  and affective local-global graph  $\mathcal{G}_a$  respectively.

For model training, the maximum training epoch of the first stage is 25 while the one for stage II is 5 instead. SGD optimizer is utilized to optimize the training process with the initial learning rate being 1e-2 and momentum being 0.9. A learning rate scheduler is also applied with the step being 10. The learning rate of the second training stage is 1e-3. Cross-entropy loss is selected as the loss function to guide the training process. For more details, please refer to the open-access GitHub repository for LGG.

## 5 RESULTS AND ANALYSIS

In this section, the results of leave-one-trial-out cross-validation on the DEAP dataset will be provided and analyzed. We first show the accuracies and standard deviations (std), which will be statistically analyzed. Extensive analyses will be conducted to understand LGG better. Then saliency maps are utilized to visualize the most informative region of the data identified by LGG. Note that the LGG used in all the further analyses is LGG-A because LGG-A achieves the highest classification accuracies.

2. <https://github.com/yi-ding-cs/LGG>

### 5.1 Statistical Analysis

The classification results in terms of accuracy and standard deviation (std) on the DEAP dataset are shown in Table 2. The detailed accuracies for each subject are shown in Fig. 4-6. The two-tailed Wilcoxon Signed-Rank Test is utilized for the statistical analysis. According to the results, all deep learning methods achieve better classification results than the compared traditional machine learning methods, which shows the superior of deep learning for EEG emotion recognition. The accuracies of FBFgMDM, FBTSC, and Unsupervised learning are all below 70% which is a commonly used threshold of performance evaluation in the BCI domain [22]. LGG with the affective local-global graph (LGG-A) achieves the best classification accuracies for all three dimensions, with the accuracies being 80.90% for arousal, 69.34% for valence, and 81.88% for liking. When the general local-global graph is utilized for LGG (LGG-G), the performances become worse. Compared with LGG-G, LGG-A has 1.31% improvement for arousal, 3.66% improvement for valence, and 3.18% increment for liking, respectively. The accuracies of LGG-A for arousal, valence, and liking are 3.53% ( $p < 0.05$ ), 3.28% ( $p = 0.1310$ ), and 4.88% ( $p < 0.05$ ) higher than the ones of TSception (the third-highest method among all). EEGNet achieves 74.03% for arousal, 66.25% for valence, and 76.71% for liking, which are 6.87% ( $p < 0.001$ ), 3.09% ( $p = 0.1141$ ), and 5.17% ( $p < 0.05$ ) lower than LGG-A. The accuracies of ShallowConvNet are 72.39%, 63.02%, and 74.01% for arousal, valence, and liking, which are significantly lower than LGG-A with the accuracies being 8.51% ( $p < 0.001$ ), 6.32% ( $p < 0.05$ ), and 7.87% ( $p < 0.001$ ) lower than the ones of LGG-A. DeepConvNet shows the lowest classification accuracies among all the deep learning methods, which has 8.69% ( $p < 0.001$ ), 6.54% ( $p < 0.05$ ), and 7.55% ( $p < 0.001$ ) lower accuracies than LGG-A for arousal, valence, and liking. The accuracies of all the deep learning methods are high for arousal and liking while the accuracies for valence are relatively lower than the other two dimensions, which indicates the valence state is harder to predict.

TABLE 3  
Number of subjects with ACC > 70%

Method	Arousal	Valence	Liking
DeepConvNet	20	8	20
ShallowConvNet	18	11	22
EEGNet	21	14	24
TSception	22	11	21
<b>LGG-A</b>	<b>24</b>	<b>14</b>	<b>27</b>

There are 32 subjects in the DEAP dataset.

The number of subjects whose classification accuracies are higher than 70% using different methods is also analyzed because 70% is a common threshold for a BCI system to be used in real-world applications in the BCI field [22]. The results are shown in Table 3. LGG has the most number of subjects who have accuracies higher than 70% for all three dimensions (24 for arousal, 14 for valence, and 27 for liking), which performances better than other methods, except valence dimension for which LGG has the same number as EEGNet.



To further analyze the classification performances, the mean accuracy of top and bottom 25% subjects using different methods are also shown in Table 4. According to Table 4 (a), TSception has the highest averaged accuracy (62.25%) of the bottom 25% for arousal, while LGG-A achieves a 99.11% averaged accuracy of the top 25% which is the best compared with the others. LGG-A has the highest accuracies of both bottom and top 25% for valence and liking, with 52.00% and 89.01% for the bottom and top 25% for valence, 57.02% and 99.58% for the bottom and top 25% for liking, respectively.

## 5.2 Ablation Study

The proposed method LGG has several components. In order to better understand the network, several ablation studies are conducted to understand: 1) the contribution of local graph filtering; 2) the contribution of global graph filtering. The ablation study results will be discussed. Each component is removed from the LGG model one by one, and the new classification accuracies and the performance changes are reflected in Table 5.

### 5.2.1 The Contribution of Local Graph Filtering

The local graph-filtering layer learns from each local graph and outputs the embedding of each local graph. The local graph filtering is operated on each local graph. The learned embedding will become the node attribute in the global graph. To understand the contribution of the local graph-filtering layer, it is removed from LGG. In this case, each EEG channel is one node in the graph, and the learnable adjacent matrix,  $A_{global} \in \mathbb{R}^{n \times n}$ , reflects the connection among all the nodes ( $n$  is the number of EEG electrodes).

After removing the local graph-filtering part of LGG, the results for three dimensions are shown in the first row of Table 5. After removing the local graph-filtering layer entirely, the accuracies drop for all three dimensions. For arousal, the accuracy drops from 80.90% to 77.50%, decreasing by 3.40%. For valence, the accuracy drops by 1.46%. A more significant drop (4.41%) is observed for liking. The drops indicate the importance of the local graph-filtering layer, especially for arousal and liking.

### 5.2.2 Contribution of Global Graph Filtering

In LGG, the global graph filtering is utilized on the learned local-graph embeddings, with the adjacent matrix being learnable. It is designed to learn the complex relations among different functional areas of the brain during high-level cognitive processes [26]. It is removed from the LGG to analyze its importance to the classification performance. In this situation, only the local graph-filtering layer is kept to learn the spatial pattern of EEG. After getting the embeddings of local graphs, the latent representation will be fed into fully connected layers without global graph filtering.

According to the second row of Table 5, the accuracies all drop after removing the global graph-filtering layer. And the decreases are higher than the ones without the local graph-filtering layer. A 9.99% drop is observed for arousal after discarding the global graph-filtering layer, while the one for valence is 8.54%. The largest drop is for the liking dimension being 12.90%. The smallest drop (8.54% for valence) after

removing global graph filtering is higher than the largest one (4.41% for liking) when local graph filtering is removed. The results show the importance of global graph filtering in LGG.

## 5.3 Effects of The Number of T Kernels in Temporal Convolutional Layer

EEG signals consist of very distinct temporal information [25]. The temporal information is learned by multi-scale 1D convolutional kernels (T kernels) in the time dimension. The well-learned temporal representations are crucial for the success of spatial learning using graph neural networks. To study the effect of the number of T kernels in the temporal convolutional layer, the number of T kernels is set from [5, 10, 15, 20, 25].

The results are shown in Table 6. The accuracies on both test and validation set are reported since the validation set is utilized for hyper-parameters selection. The highest accuracies for both arousal and liking are achieved when the number of T kernels is 5 in the temporal convolutional layer, with the accuracies being 80.90% for arousal and 81.88% for liking on test data. But for valence, the best accuracy (70.31%) is observed when there are 10 T kernels in the first convolutional layer. From the results, a relatively smaller number of kernels are preferred. Because with no significant difference in terms of accuracy, fewer kernels will give fewer trainable parameters of the neural network.

## 5.4 Effects of Different Local-Global-Graph Definitions

The success of LGG relies on well-defined local-global graphs. Prior knowledge of neuroscientific evidence is involved in the graph structure design. The general local-global graph in Fig. 2 is designed according to the 10-20 system, which measures the activities of different functional areas in the brain. For the affective local-global graph (in Fig. 3), frontal asymmetry of the emotional cognitive process [27] is further considered. We add several left and right frontal sub-graphs to the general local-global graph. The left and right areas can refer to [40], in which the left and right areas are defined for all brain functional areas. We only adopt the left and right areas in the frontal area for the affective local-global graph since neuroscience evidence [28] shows the asymmetry pattern appears in the frontal area. Hence in this part, the graph structure in [40] is also compared with two local-global graphs proposed in this paper. Fig. 7 shows the three compared local-global graphs. The subareas of Fig. 7 (c) are symmetrically located on right and left hemispheres so it is named hemisphere.

From the results in Table 7, the LGG using affective local-global graph ( $\mathcal{G}_a$ ) achieves the best classification accuracies for all three dimensions. Compared with the general local-global graph,  $\mathcal{G}_g$ , the symmetric local graphs provide more information in the frontal area, especially for the asymmetric pattern in the emotional process of the brain [27]. The accuracies of LGG using  $\mathcal{G}_a$  are 1.31%, 3.66%, and 3.18% higher than the ones using  $\mathcal{G}_g$ . It indicates the effectiveness of the frontal symmetric local area design.

The difference between  $\mathcal{G}_a$  and  $\mathcal{G}_h$  [40] is the  $\mathcal{G}_h$  has symmetric local areas on the left and right hemispheres, instead of having symmetric local areas only on the frontal

TABLE 4  
Mean accuracy of top and bottom 25% subjects on DEAP

method	Bottom 25%	Top 25%	method	Bottom 25%	Top 25%	method	Bottom 25%	Top 25%
DeepCN	53.96%	88.31%	DeepCN	49.40%	79.06%	DeepCN	58.22%	91.39%
ShallowCN	58.38%	87.43%	ShallowCN	48.51%	78.30%	ShallowCN	56.19%	89.93%
EEGNet	54.38%	91.70%	EEGNet	48.55%	82.85%	EEGNet	57.83%	93.57%
TSception	<b>62.25%</b>	95.01%	TSception	50.61%	83.19%	TSception	54.74%	95.59%
LGG-A	59.41%	<b>99.11%</b>	LGG-A	<b>52.00%</b>	<b>89.01%</b>	LGG-A	<b>57.02%</b>	<b>99.58%</b>

(a) Arousal

(b) Valence

(c) Liking

DeepCN: DeepConvNet; ShallowCN: ShallowConvNet.

TABLE 5  
Results of ablation study of local and global graph-filtering in LGG on DEAP

Local graph filtering	Global graph filtering	Arousal	changes	Valence	changes	Liking	changes
	✓	77.50%	-3.40%	67.88%	-1.46%	77.47%	-4.41%
✓		70.91%	-9.99%	60.80%	-8.54%	68.98%	-12.90%
✓	✓	<b>80.90%</b>	-	<b>69.34%</b>	-	<b>81.88%</b>	-

✓: keep the component.

changes: compared with the original LGG-A.

TABLE 6  
Effect of T kernel numbers

Num	Test			Validation		
	Arousal	Valence	Liking	Arousal	Valence	Liking
5	<b>80.90%</b>	69.34%	<b>81.88%</b>	<b>87.35%</b>	79.83%	<b>88.24%</b>
10	79.51%	<b>70.31%</b>	79.77%	85.97%	<b>80.59%</b>	86.49%
15	75.70%	63.32%	76.83%	86.03%	79.10%	86.10%
20	80.41%	66.75%	81.63%	87.03%	79.69%	87.07%
25	77.13%	66.50%	80.16%	87.32%	79.30%	87.70%

The test accuracy is the mean accuracy of the leave-one-trial-out cross-validation.

The validation accuracy is the mean accuracy of the inner 5-fold cross-validation.

TABLE 7  
Effects of different local-global graph definitions

Type	Arousal	Valence	Liking
hemisphere	78.66%	64.21%	77.58%
general	79.59%	65.68%	78.70%
<b>affective</b>	<b>80.90%</b>	<b>69.34%</b>	<b>81.88%</b>

area in  $\mathcal{G}_a$ . Using  $\mathcal{G}_a$ , LGG shows 2.24%, 5.13%, and 4.3% improvements over the one using  $\mathcal{G}_h$ . The results show the superiority of the affective local-global-graph design which takes the advantage of the psychophysiological evidence [27] that the right and left half of the frontal brain areas are asymmetrically related to the emotional process.

## 5.5 Interpretability and Visualization

In this part, the saliency map [32] is utilized to visualize which parts of the data are more informative. To better visualize the saliency map, the original saliency map is averaged along the time dimension to get the topological map of the EEG channels for each subject. Fig. 8 shows the

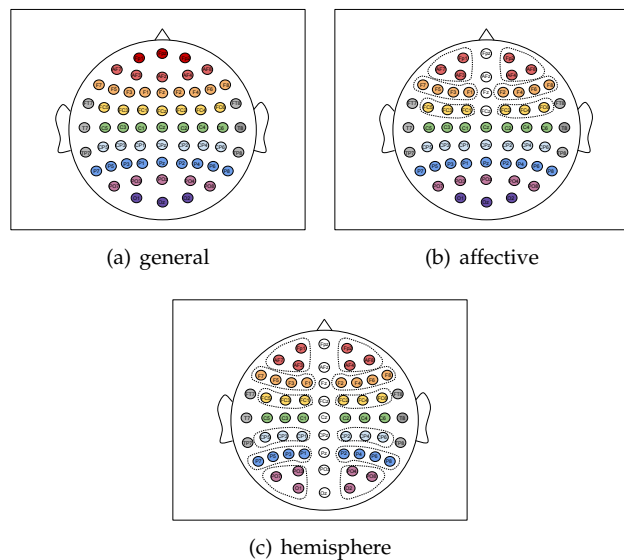


Fig. 7. Different definitions of local-global graphs. (a) and (b) are the proposed general and affective local-global graphs, which are introduced in Section A of Chapter III. (c) is utilized in [40], which has subareas from frontal to occipital lobe. The subareas of (c) are symmetrically located on right and left hemisphere therefore it is named hemisphere.

averaged saliency map of all the subjects. From the figure, LGG learns more from the frontal and temporal areas of the brain. The frontal area of the brain is full of emotional information [9] [44]. The temporal lobe of the brain has relations to the emotional process [45]. Besides, neuroscience evidence [46] suggests the temporal lobe has a crucial role in the formation of melody representations, which is closely related to the stimuli (music videos) used in the DEAP dataset. The above neurological knowledge indicates the neural network learns from the emotion-related regions of EEG signals.

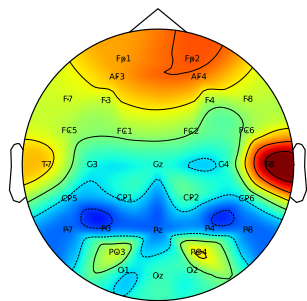


Fig. 8. Averaged saliency map of all 32 subjects in DEAP. LGG learns more information from frontal and temporal areas which are in orange and red in the figure. The names of EEG electrodes are also plotted for better visualization.

## 6 DISCUSSION

The human brain can be modeled as a complex network with a hierarchical spatial and functional organization at the level of neurons, local circuits, and functional areas. Involving neuroscientific knowledge in neural network design has huge potentials to improve the decoding performance of deep learning. To improve the brain activity decoding ability of deep learning, we propose LGG, a local-global graph neural network that can model the brain activities within and between different functional areas of the brain as well as the complex relations among them during the cognitive processes. We evaluate the effectiveness of the proposed method in emotion recognition tasks using brain signals.

It can be seen from all the experiment results that LGG can effectively learn from the local-global-graph representation of EEG, yielding the best classification accuracies for all three emotional dimensions. When we conduct the experiments, testing data leakage, biased evaluation, and chance level shifting caused by unbalanced classes are considered and avoided to form a robust and generalized evaluation. If one trial’s data is cropped into short segments and randomly shuffled before dividing the data into training and testing data, an overestimated accuracy can be achieved with the sacrifice of generalization [1]. Because the data within each trial is very similar, randomly shuffle will cause testing data leakage issues so that an overestimated accuracy will be observed [14]. The entire trial is utilized as the input of the classifier, and a leave-one-trial-out cross-validation is adopted for each subject as [31] to avoid the above issues. Subject-specific experiments are conducted as [14]. In deep learning, hyper-parameters need to be selected. The nested cross-validation [42] is further utilized with its outer loop being leave-one-trial-out and its inner loop being 5-fold cross-validation so that testing data leakage and biased evaluation problems are avoided. Because the hyper-parameters are selected according to the performance on the validation set of the inner loop as [14] suggested. The two-stage training process helps to take the full usage of the training data while isolating the testing data from training. Following the suggestion of [31], we solved the unbalanced class issue by randomly duplicated the trials of the less-sample class to avoid the chance level shifting issue

in accuracy.

LGG is a neurologically inspired neural network. Two local-global-graph representations of EEG are proposed to represent the complex relations during cognitive processes in the brain. There are several functional areas that are related to certain brain functions [26]. The local graphs in the general local-global graph,  $\mathcal{G}_g$ , is designed to represent the activities of the different functional area of the brain. The global connections among local graphs are proposed to learn the complex relations among them since some functional areas will be activated together during cognitive processes [28]. The frontal asymmetry during the emotional process [27] is further applied to the local-global graph design so we add sub-graphs symmetrically located on the left and right frontal area in the affective local-global graph ( $\mathcal{G}_a$ ). According to Table 2, LGG-A achieves the best performance with the accuracies being 80.90% for arousal, 69.34% for valence, and 81.88% for liking, while the LGG-G achieves second place among all the compared methods. This indicates the effectiveness of the local-global-graph designs. From Table 5, global graph filtering is more important than local graph filtering because the accuracy drops of removing global graph filtering are much larger than the ones of removing local graph filtering. This also indicates the effectiveness of the neuroscience [28] that activating one region tends to activate other regions during the emotional process. Removing either of the local and global graph-filtering layers leads to the downgrade of the classification performance. This shows the combination of two types of graph-filtering layers leads to the success of LGG. We also analyzed the effect of the number of the T kernels in the temporal convolutional layer. The results in Table 6 show that a smaller number of kernels can learn effectively from EEG graphs. This might because of the kernel-level attention fusion which will lead the network to learn the most important information from different kernels. We only add the symmetrical local graphs in the frontal area according to the neuroscience knowledge [28] that emotion asymmetry appears particularly within the frontal area. We also evaluate the graph from [40] which has subareas from frontal to occipital lobe. From Table 7, the accuracies of LGG using  $\mathcal{G}_a$  are 1.31%, 3.66%, and 3.18% higher than the ones of LGG using  $\mathcal{G}_g$ , which shows the effectiveness of adding frontal symmetric local graphs. LGG using  $\mathcal{G}_a$  shows 2.24%, 5.13%, and 4.3% higher accuracies than the one using  $\mathcal{G}_h$ . This indicates adding symmetric local graphs in the frontal area only is better than adding them on the whole brain, which is consistent with neuroscience [28]. Furthermore, the averaged saliency map of all subjects in Fig. 8 shows LGG learns more emotional information from frontal and temporal regions. According to [44] [9], the frontal area has strong relations with emotional processes. Besides, LGG gets more information about the emotional state of the brain from the temporal lobe, which is consistent with the neuroscience knowledge [45] that the temporal lobe also has relations with emotional processes. We also notice that the temporal lobe plays an important role in the formation of melody representations [46], and emotional memory retrieval [47]. It also supports our findings that LGG learns from the proper regions of the EEG because the stimuli used in DEAP are music videos.

Although LGG achieves the highest classification accuracies for emotion recognition tasks, the limitation of this work should also be noticed. The first one is relatively low accuracy for the valence dimension. Compared with the accuracies for arousal (80.90%) and liking (81.88%), the one for valence is lower (69.34%). Besides, in this work, the nodes within each local area are set to be fully connected, which might not be able to reflect the complex brain activities inside that functional area. How to model the relations within local areas should be explored. Further improvement of the network or loss function design should be considered in the future to improve the classification performance.

## 7 CONCLUSION

In this paper, we propose LGG, a neurologically inspired graph neural network, to learn from local-global-graph representations of EEG. Multi-scale 1D temporal convolutional kernels with kernel-level attention fusion are utilized to learn the temporal dynamics of EEG. Local and global graph filtering learn the brain activities within each functional area and the complex relations among them during the cognitive process in the brain, respectively. With a robust nested cross-validation strategy, the proposed method and several state-of-the-art methods are evaluated on the publicly available benchmark dataset. The proposed method achieves significantly ( $p < 0.05$ ) higher accuracies than other methods. Further analyses also show the effectiveness of applying neurological knowledge into network design.

## ACKNOWLEDGMENTS

This work was partially supported by the RIE2020 AME Programmatic Fund, Singapore (No. A20G8b0102).

## REFERENCES

- [1] X. Zhang, J. Liu, J. Shen, S. Li, K. Hou, B. Hu, J. Gao, T. Zhang, and B. Hu, "Emotion recognition from multimodal physiological signals using a regularized deep fusion of kernel machine," *IEEE Transactions on Cybernetics*, pp. 1–14, 2020.
- [2] F. Lotte and C. Guan, "Regularizing common spatial patterns to improve BCI designs: unified theory and new algorithms," *IEEE Transactions on Biomedical Engineering*, vol. 58, no. 2, pp. 355–362, 2010.
- [3] R. Liu, Y.-X. Wang, and L. Zhang, "An FDES-based shared control method for asynchronous brain-actuated robot," *IEEE Transactions on Cybernetics*, vol. 46, no. 6, pp. 1452–1462, 2015.
- [4] R. Foong, K. K. Ang, C. Quek, C. Guan, K. S. Phua, C. W. K. Kuah, V. A. Deshmukh, L. H. L. Yam, D. K. Rajeswaran, N. Tang *et al.*, "Assessment of the efficacy of eeg-based MI-BCI with visual feedback and EEG correlates of mental fatigue for upper-limb stroke rehabilitation," *IEEE Transactions on Biomedical Engineering*, vol. 67, no. 3, pp. 786–795, 2019.
- [5] V. Zotev, A. Mayeli, M. Misaki, and J. Bodurka, "Emotion self-regulation training in major depressive disorder using simultaneous real-time fMRI and EEG neurofeedback," *NeuroImage: Clinical*, vol. 27, p. 102331, 2020.
- [6] J. K. Carpenter, L. A. Andrews, S. M. Witcraft, M. B. Powers, J. A. J. Smits, and S. G. Hofmann, "Cognitive behavioral therapy for anxiety and related disorders: A meta-analysis of randomized placebo-controlled trials," *Depression and Anxiety*, vol. 35, no. 6, pp. 502–514, 2018.
- [7] D. M. Fresco, D. S. Mennin, R. G. Heimberg, and M. Ritter, "Emotion regulation therapy for generalized anxiety disorder," *Cognitive and Behavioral Practice*, vol. 20, no. 3, pp. 282 – 300, 2013.
- [8] L. Greenberg, "Emotion-focused therapy," *Clinical Psychology & Psychotherapy*, vol. 11, no. 1, pp. 3–16, 2004.
- [9] S. M. Alarcão and M. J. Fonseca, "Emotions recognition using EEG signals: A survey," *IEEE Transactions on Affective Computing*, vol. 10, no. 3, pp. 374–393, July 2019.
- [10] A. Craik, Y. He, and J. L. Contreras-Vidal, "Deep learning for electroencephalogram (EEG) classification tasks: a review," *Journal of Neural Engineering*, vol. 16, no. 3, p. 031001, apr 2019.
- [11] W. Zheng, J. Zhu, and B. Lu, "Identifying stable patterns over time for emotion recognition from EEG," *IEEE Transactions on Affective Computing*, vol. 10, no. 3, pp. 417–429, July 2019.
- [12] P. Li, H. Liu, Y. Si, C. Li, F. Li, X. Zhu, X. Huang, Y. Zeng, D. Yao, Y. Zhang, and P. Xu, "EEG based emotion recognition by combining functional connectivity network and local activations," *IEEE Transactions on Biomedical Engineering*, vol. 66, no. 10, pp. 2869–2881, Oct 2019.
- [13] X. Li, D. Song, P. Zhang, Y. Zhang, Y. Hou, and B. Hu, "Exploring EEG features in cross-subject emotion recognition," *Frontiers in Neuroscience*, vol. 12, p. 162, 2018.
- [14] Z. Liang, S. Oba, and S. Ishii, "An unsupervised EEG decoding system for human emotion recognition," *Neural Networks*, vol. 116, pp. 257 – 268, 2019.
- [15] R. T. Schirrmester, J. T. Springenberg, L. D. J. Fiederer, M. Glasstetter, K. Eggenesperger, M. Tangermann, F. Hutter, W. Burgard, and T. Ball, "Deep learning with convolutional neural networks for EEG decoding and visualization," *Human Brain Mapping*, vol. 38, no. 11, pp. 5391–5420, 2017.
- [16] O. Kwon, M. Lee, C. Guan, and S. Lee, "Subject-independent brain-computer interfaces based on deep convolutional neural networks," *IEEE Transactions on Neural Networks and Learning Systems*, pp. 1–14, 2019.
- [17] Y. R. Tabar and U. Halici, "A novel deep learning approach for classification of EEG motor imagery signals," *Journal of Neural Engineering*, vol. 14, no. 1, p. 016003, nov 2016.
- [18] V. J. Lawhern, A. J. Solon, N. R. Waytowich, S. M. Gordon, C. P. Hung, and B. J. Lance, "EEGNet: a compact convolutional neural network for EEG-based brain-computer interfaces," *Journal of Neural Engineering*, vol. 15, no. 5, p. 056013, Jul 2018.
- [19] J. Li, Z. Zhang, and H. He, "Hierarchical convolutional neural networks for EEG-based emotion recognition," *Cognitive Computation*, vol. 10, no. 2, pp. 368–380, Apr 2018.
- [20] Y. Li, W. Zheng, Y. Zong, Z. Cui, T. Zhang, and X. Zhou, "A bi-hemisphere domain adversarial neural network model for EEG emotion recognition," *IEEE Transactions on Affective Computing*, pp. 1–1, 2018.
- [21] Y. Ding, N. Robinson, Q. Zeng, D. Chen, A. A. Phyo Wai, T. S. Lee, and C. Guan, "Tsception: a deep learning framework for emotion detection using eeg," in *2020 International Joint Conference on Neural Networks (IJCNN)*, 2020, pp. 1–7.
- [22] F. Fahimi, Z. Zhang, W. B. Goh, T.-S. Lee, K. K. Ang, and C. Guan, "Inter-subject transfer learning with an end-to-end deep convolutional neural network for EEG-based BCI," *Journal of Neural Engineering*, vol. 16, no. 2, p. 026007, Jan 2019.
- [23] Z. Jiao, X. Gao, Y. Wang, J. Li, and H. Xu, "Deep convolutional neural networks for mental load classification based on EEG data," *Pattern Recognition*, vol. 76, pp. 582 – 595, 2018.
- [24] Y. Yang, Q. M. J. Wu, W. Zheng, and B. Lu, "EEG-based emotion recognition using hierarchical network with subnetwork nodes," *IEEE Transactions on Cognitive and Developmental Systems*, vol. 10, no. 2, pp. 408–419, June 2018.
- [25] Kai Keng Ang, Zheng Yang Chin, Haihong Zhang, and Cuntai Guan, "Filter bank common spatial pattern (FBCSP) in brain-computer interface," in *2008 IEEE International Joint Conference on Neural Networks (IEEE World Congress on Computational Intelligence)*, June 2008, pp. 2390–2397.
- [26] J. Power, A. Cohen, S. Nelson, G. Wig, K. Barnes, J. Church, A. Vogel, T. Laumann, F. Miezin, B. Schlaggar, and S. Petersen, "Functional network organization of the human brain," *Neuron*, vol. 72, no. 4, pp. 665 – 678, 2011.
- [27] J. J. B. Allen, P. M. Keune, M. Schönenberg, and R. Nusslock, "Frontal EEG alpha asymmetry and emotion: From neural underpinnings and methodological considerations to psychopathology and social cognition," *Psychophysiology*, vol. 55, no. 1, p. e13028, 2018.
- [28] H. Kober, L. F. Barrett, J. Joseph, E. Bliss-Moreau, K. Lindquist, and T. D. Wager, "Functional grouping and cortical-subcortical interactions in emotion: A meta-analysis of neuroimaging studies," *NeuroImage*, vol. 42, no. 2, pp. 998 – 1031, 2008.

- [29] T. Song, W. Zheng, P. Song, and Z. Cui, "EEG emotion recognition using dynamical graph convolutional neural networks," *IEEE Transactions on Affective Computing*, vol. 11, no. 3, pp. 532–541, 2020.
- [30] S. Koelstra, C. Muhl, M. Soleymani, J. Lee, A. Yazdani, T. Ebrahimi, T. Pun, A. Nijholt, and I. Patras, "DEAP: A database for emotion analysis ;using physiological signals," *IEEE Transactions on Affective Computing*, vol. 3, no. 1, pp. 18–31, 2012.
- [31] A. Appriou, A. Cichocki, and F. Lotte, "Modern machine-learning algorithms: For classifying cognitive and affective states from electroencephalography signals," *IEEE Systems, Man, and Cybernetics Magazine*, vol. 6, no. 3, pp. 29–38, 2020.
- [32] K. Simonyan, A. Vedaldi, and A. Zisserman, "Deep inside convolutional networks: Visualising image classification models and saliency maps," *arXiv preprint arXiv:1312.6034*, 2013.
- [33] N. Robinson, S. Lee, and C. Guan, "EEG representation in deep convolutional neural networks for classification of motor imagery," in *2019 IEEE International Conference on Systems, Man and Cybernetics (SMC)*, Oct 2019, pp. 1322–1326.
- [34] S. Siddharth, T. Jung, and T. J. Sejnowski, "Utilizing deep learning towards multi-modal bio-sensing and vision-based affective computing," *IEEE Transactions on Affective Computing*, pp. 1–1, 2019.
- [35] S. Jang, S. Moon, and J. Lee, "EEG-based video identification using graph signal modeling and graph convolutional neural network," in *2018 IEEE International Conference on Acoustics, Speech and Signal Processing (ICASSP)*, 2018, pp. 3066–3070.
- [36] P. Zhong, D. Wang, and C. Miao, "EEG-based emotion recognition using regularized graph neural networks," *IEEE Transactions on Affective Computing*, pp. 1–1, 2020.
- [37] F. Scarselli, M. Gori, A. C. Tsoi, M. Hagenbuchner, and G. Monfardini, "The graph neural network model," *IEEE Transactions on Neural Networks*, vol. 20, no. 1, pp. 61–80, Jan 2009.
- [38] M. Defferrard, X. Bresson, and P. Vandergheynst, "Convolutional neural networks on graphs with fast localized spectral filtering," in *Advances in Neural Information Processing Systems 29*, 2016, pp. 3844–3852.
- [39] T. N. Kipf and M. Welling, "Semi-supervised classification with graph convolutional networks," *Proc. of ICLR*, 2017.
- [40] R. Grabner and B. De Smedt, "Oscillatory EEG correlates of arithmetic strategies: A training study," *Frontiers in Psychology*, vol. 3, p. 428, 2012.
- [41] S. Ioffe and C. Szegedy, "Batch normalization: Accelerating deep network training by reducing internal covariate shift," in *Proceedings of the 32nd International Conference on Machine Learning*, ser. Proceedings of Machine Learning Research, vol. 37, 07–09 Jul 2015, pp. 448–456.
- [42] S. Varma and R. Simon, "Bias in error estimation when using cross-validation for model selection," *BMC Bioinformatics*, vol. 7, no. 1, p. 91, 2006.
- [43] A. Paszke, S. Gross, F. Massa, A. Lerer, J. Bradbury, G. Chanan, T. Killeen, Z. Lin, N. Gimelshein, L. Antiga, A. Desmaison, A. Kopf, E. Yang, Z. DeVito, M. Raison, A. Tejani, S. Chilamkurthy, B. Steiner, L. Fang, J. Bai, and S. Chintala, "PyTorch: An imperative style, high-performance deep learning library," in *Advances in Neural Information Processing Systems 32*, 2019, pp. 8024–8035.
- [44] P. A. Kragel, M. Kano, L. Van Oudenhove, H. G. Ly, P. Dupont, A. Rubio, C. Delon-Martin, B. L. Bonaz, S. B. Manuck, P. J. Gianaros *et al.*, "Generalizable representations of pain, cognitive control, and negative emotion in medial frontal cortex," *Nature neuroscience*, vol. 21, no. 2, pp. 283–289, 2018.
- [45] I. R. Olson, A. Plotzker, and Y. Ezzyat, "The enigmatic temporal pole: a review of findings on social and emotional processing," *Brain*, vol. 130, no. 7, pp. 1718–1731, 2007.
- [46] L. Jäncke, "Music, memory and emotion," *Journal of biology*, vol. 7, no. 6, pp. 1–5, 2008.
- [47] R. J. Dolan, R. Lane, P. Chua, and P. Fletcher, "Dissociable temporal lobe activations during emotional episodic memory retrieval," *Neuroimage*, vol. 11, no. 3, pp. 203–209, 2000.